Journal of Saudi Chemical Society (2017) **21**, S275–S282

King Saud University

Journal of Saudi Chemical Society

www.ksu.edu.sa
www.sciencedirect.com

ORIGINAL ARTICLE

Surfactant-free hydrothermal synthesis, growth mechanism and photocatalytic properties of $PbMoO_4$ polyhedron microcrystals

Lei Zhang, Dianrang Bai, Min Zhou, Chengling Pan *

Laboratory of Multiscale Materials and Molecular Catalysis, School of Materials Science and Engineering, Anhui University of Science and Technology, Huainan, Anhui 232001, People's Republic of China

Received 21 January 2014; revised 27 February 2014; accepted 2 March 2014
Available online 18 March 2014

KEYWORDS

Semiconductors;
Crystal growth;
Microstructure;
Photocatalytic properties

Abstract In the present paper, $PbMoO_4$ polyhedron microcrystals were prepared via a facile hydrothermal synthetic route in the absence of any surfactant, employing $Pb(NO_3)_2$ and $Na_2MoO_4 \cdot 2H_2O$ as starting materials. The phase and morphology of the product were characterized by powder X-ray diffraction (XRD), energy dispersive spectrometry (EDS), Raman spectrum, FT-IR spectroscopy and scanning electron microscopy (SEM). Some factors influencing the morphology of the final product have been investigated. Experimental results indicated that appropriate volume of glycerol could effectively regulate the nucleation rate and contribute to the formation of $PbMoO_4$ microcrystals of large size. A possible growth mechanism of the $PbMoO_4$ polyhedron was proposed based on the experimental results. Moreover, the photocatalytic properties of the products were studied.

1. Introduction

Metal molybdate materials with scheelite-type tetragonal structure exhibit interesting optical, electronic and magnetic properties and thus have great potential applications in fields such as photoluminescent materials, microwave devices, optical fibers, scintillator materials, humidity sensors, and catalysis [6,31,26,27]). As one of the members, $PbMoO_4$ has attracted considerable attention and has been widely used in optical-instrument engineering, photoconductivity and as a UV-light-driven photocatalyst [14,8,9]. Traditionally, $PbMoO_4$ is prepared via high temperature solid-state reactions. In recent years, several solution-phase routes have been employed to controllably prepare this family of materials [5,1,2,12,13,10]. For example, Shen et al. have designed a facile CTAB-assisted hydrothermal process to prepare $PbMoO_4$ microcrystals with preferentially exposed (001) facets [15]. Xing et al. reported the successful preparation of well-defined and uniform $PbMoO_4$ polyhedral crystals via a microemulsion-based solvothermal method [21]. Usually, organic surfactants are introduced to the reaction medium and served as templates or structure directing agents in these synthetic processes, which

* Corresponding author. Tel./fax: +86 554 6668649.
E-mail address: clpan@aust.edu.cn (C. Pan).
Peer review under responsibility of King Saud University.

Production and hosting by Elsevier

http://dx.doi.org/10.1016/j.jscs.2014.03.002

can effectively modulate the growth of the structure and morphology of the products. In most cases, the pure product is obtained only after the complete removal of the surfactants. Therefore, it makes the experimental process more complicated. In addition, most of the organic surfactants are high in cost. However, up to now, reports on the preparation of $PbMoO_4$ polyhedron microcrystals in the absence of any surfactant remain uncommon.

Herein, we report a facile surfactant-free solution-phase synthetic approach for the preparation of the $PbMoO_4$ polyhedron. By controlling the experimental parameters, such as reaction time, temperature and the volume ratio of water and glycerol, the $PbMoO_4$ polyhedron has been successfully fabricated. A possible growth mechanism of the product is proposed. In addition, the photocatalytic properties of the products were studied.

2. Materials and methods

All reagents were purchased from the Shanghai Chemical Company and used without further purification. In a typical preparation procedure, $Pb(NO_3)_2$ (0.001 mol) was dissolved in 5 mL of deionized water and 20 mL of glycerol. Then, 5 mL of deionized water containing 0.001 mol of $Na_2MoO_4 \cdot 2H_2O$ was slowly dropped into the above solution. The as-obtained solution was stirred for 10 min and transferred into a stainless-steel autoclave with a Teflon liner of 40 mL capability. After treating the mixture at 180 °C for 24 h, it was cooled to room temperature naturally. The product was collected, washed with deionized water and absolute ethanol, and dried in a vacuum at 60 °C for 6 h with a yield of 90%.

The products were characterized by X-ray powder diffraction (XRD) with a Shimadzu XRD-6000 powder X-ray diffractometer with Cu Kα radiation (λ = 1.5418 Å), recorded with 2θ ranging from 10° to 80°. SEM images of the products were obtained on field emission scanning electron microanalyser (Hitachi S-4800), employing the accelerating voltage of 10 kV. Energy dispersive X-ray spectroscopy, being attached to the scanning electron microscope, was used to analyze the composition of the sample. Raman spectrum was taken at room temperature in the spectral range of 100–1000 cm^{-1} using a JY HR800 Raman spectromicroscope. FT-IR spectrum was recorded for KBr-diluted samples using a Nicolet Magna 750 IR spectrometer at wavenumbers 400–4000 cm^{-1}. The UV–vis diffusion reflectance spectrum (DRS) of the sample was analyzed with a UV–vis spectrophotometer (UV-3600, Shimadzu, Japan). The Brunauer–Emmett–Teller (BET) surface area was measured using a Micrometrics ASAP 2010. Photoluminescence spectrum was recorded employing an Edinburgh FLSP 920 fluorescence spectrophotometer at room temperature.

Photocatalytic degradation of RhB, MO or phenol aqueous solution was conducted in an XPA-photochemical reactor (Xujiang Electromech-anical Plant, Nanjing, China) equipped with a 500 W high-pressure mercury lamp. An electric fan and cycled condensate water were used to prevent thermal catalytic effects. 0.01 g of photocatalyst was introduced into each of a series of Pyrex reactors containing 30 mL of dye solution (10 mg/L) or phenol aqueous solution (20 mg/L) at room temperature under air, respectively. Before the light was turned on, the solution was continuously stirred for 60 min in the dark to ensure the establishment of an adsorption–desorption equilibrium. During irradiation, ~3 mL of the suspension was continually taken from the reactor at given time intervals. The photocatalyst powder and the polluted solution were separated by a centrifugal machine. The MO, RhB and phenol concentration were analyzed through a UV–vis spectrophotometer (UV-3600, Shimadzu, Japan). Total-organic-carbon (TOC) concentrations in the solutions were checked on a TOC analyzer (TOC-V CPH, Shimadzu, Japan).

3. Results and discussions

The composition and phase of the as-obtained sample were examined by XRD and EDS. Fig. 1a depicts the XRD pattern of the product prepared at 180 °C for 24 h. All the reflection peaks can be indexed to a pure tetragonal phase $PbMoO_4$ with calculated lattice constants of a = 5.42 Å and c = 12.10 Å, which are in good agreement with the literature values (JCPDS file Card No. 74-1075). The strong and sharp diffraction peaks imply good crystallinity of the product. No other impurity peak is detected. Additional evidence of the formation of $PbMoO_4$ came from energy dispersion X-ray analysis. Fig. 1b shows the EDS spectrum of the as-prepared product. The peaks of Pb, Mo and O can be easily found. The C peak in the spectrum can be attributed to CO_2 adsorbed by the sample. Quantitative analysis of the sample gives Pb, Mo and O molar ratio of 1.0:1.1:3.6, which is close to the $PbMoO_4$ stoichiometry. The microstructure and morphology of the product were investigated by SEM. As shown in Fig. 1c, the as-prepared product is composed of abundant $PbMoO_4$ polyhedron microcrystals with relatively good dispersion. A high magnification SEM image shown in Fig. 1d reveals that the surface of such polyhedron microcrystals is very smooth and no nanoparticles of small size are attached.

Fig. 2a shows the Raman spectra of the $PbMoO_4$ sample. The Raman peak at 873.5 cm^{-1} can be assigned to the symmetric stretching vibration mode $v_1(A_g)$ of the $[MoO_4]$ clusters in the $PbMoO_4$ crystal. The peaks at 766.7 and 748.0 cm^{-1} correspond to the anti-symmetric stretching $v_3(B_g)$ and $v_3(E_g)$ vibration modes, respectively. Two modes at 300–400 cm^{-1} are interpreted as the stronger $v_2(A_g)$ and weaker $v_4(B_g)$ of the regular $(MO_4)^{2-}$ tetrahedrons. The A_g mode at 169.9 cm^{-1} for $PbMoO_4$ is much weaker than other modes. These results are consistent with other previous reports about $PbMoO_4$ [12,21]. Fig. 2b illustrates the transmittance FTIR spectrum of $PbMoO_4$ polyhedron microcrystals at 180 °C for 24 h. Only the strong transmittance mode is observed at 720–900 cm^{-1}, which can be specified as the Mo–O anti-symmetric stretching vibration of the $[MoO_4]^{2-}$ tetrahedrons [8].

As a general nonaqueous solvent with a relatively high boiling point, glycerol has been widely used in the so-called polyol synthesis of various metal and metal chalcogenide nanoparticles [11,18,24]. In this work, when the volume of glycerol was controlled at 0, 5 and 10 mL, nanoparticles were obtained (Fig. 3a–c). On increasing the volume of glycerol to 15 mL, the bulk of the product was comprised of $PbMoO_4$ polyhedrons (Fig. 3d). In addition, some nanoparticles of small sizes were attached to the surface of these polyhedrons. If the volume of glycerol was controlled at 20 mL, $PbMoO_4$ polyhedrons with a smooth surface appeared (Fig. 1). These results indicate that appropriate volume of glycerol plays an important role in

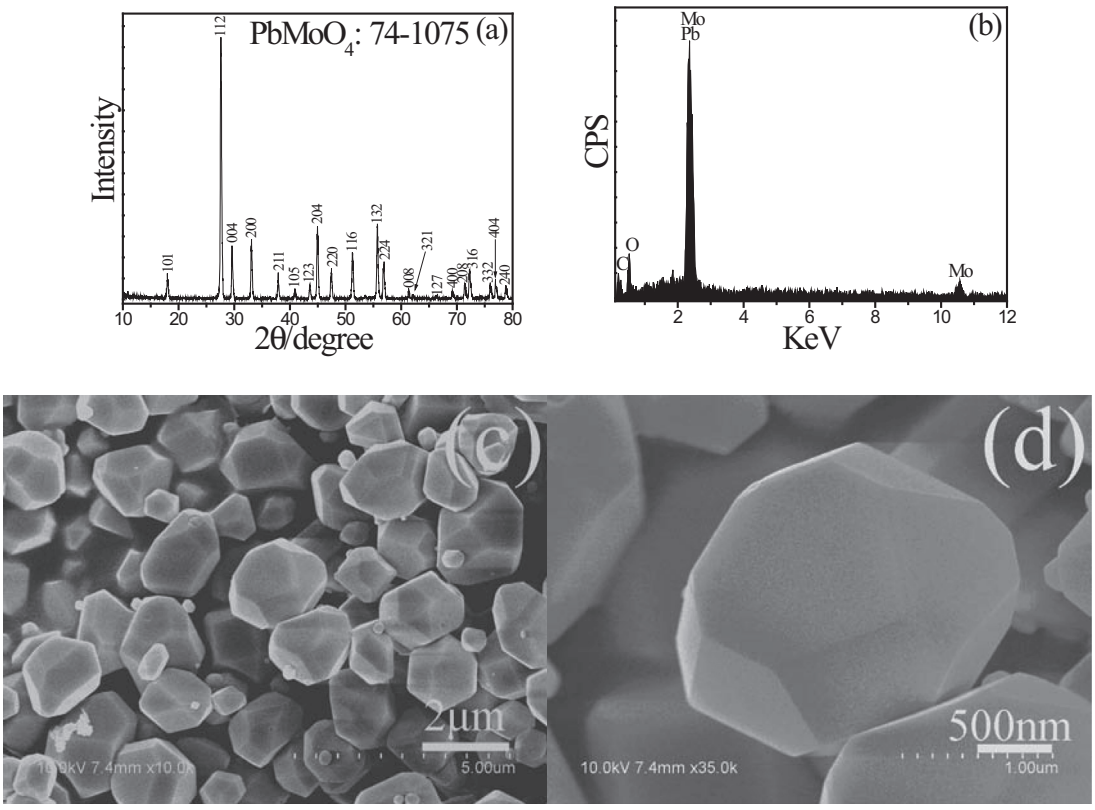

Figure 1 (a) The XRD pattern, (b) EDS spectrum and (c, d) SEM images of the as-prepared $PbMoO_4$ polyhedron microcrystals at 180 °C for 24 h.

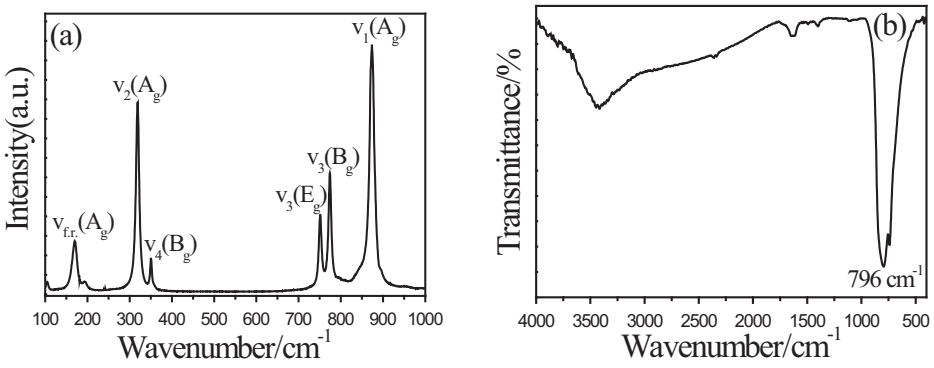

Figure 2 (a) Raman and (b) FT-IR spectra of the as-prepared $PbMoO_4$ polyhedron microcrystals at 180 °C for 24 h.

the formation of such $PbMoO_4$ polyhedrons. As is well known, a crystal growth process includes nucleation and growth. If the nucleation rate is less than the growth rate, the formation of nanoparticles of large size is favorable. Conversely, it contributes to the production of small nanoparticles [16,7]. In our reaction, when the volume of glycerol is small, nucleation stage is very easy due to the relatively low viscosity of the reaction medium. A larger number of nucleations may cause a significant reduction of the ''nutrition''. In this case, the nucleation rate should be greater than the growth rate, which result that the morphology of the product remains in the nanoparticle stage (e.g., 0, 5, 10 mL). High glycerol content increases the viscosity of the reaction system (e.g., 15, 20 mL), which can effectively regulate the nucleation rate and retain enough ''nutrition'' for the subsequent growth stage [32]. Therefore, higher growth rate leads to the formation of polyhedrons of large size.

It is found that the variation of reaction temperature greatly changes the product morphology.

When the reaction temperature was carried out at 150 °C for 24 h, $PbMoO_4$ polyhedrons and nanoparticles coexisted in the final product (Fig. 4). Compared to the experimental result controlled at 180 °C for 24 h (Fig. 1), one can find that high reaction temperature is in favor of the transformation from nanoparticles to polyhedrons.

In order to monitor the morphological evolution and reveal the possible growth mechanism of the $PbMoO_4$ polyhedrons, a series of time-dependent experiments were carefully carried out

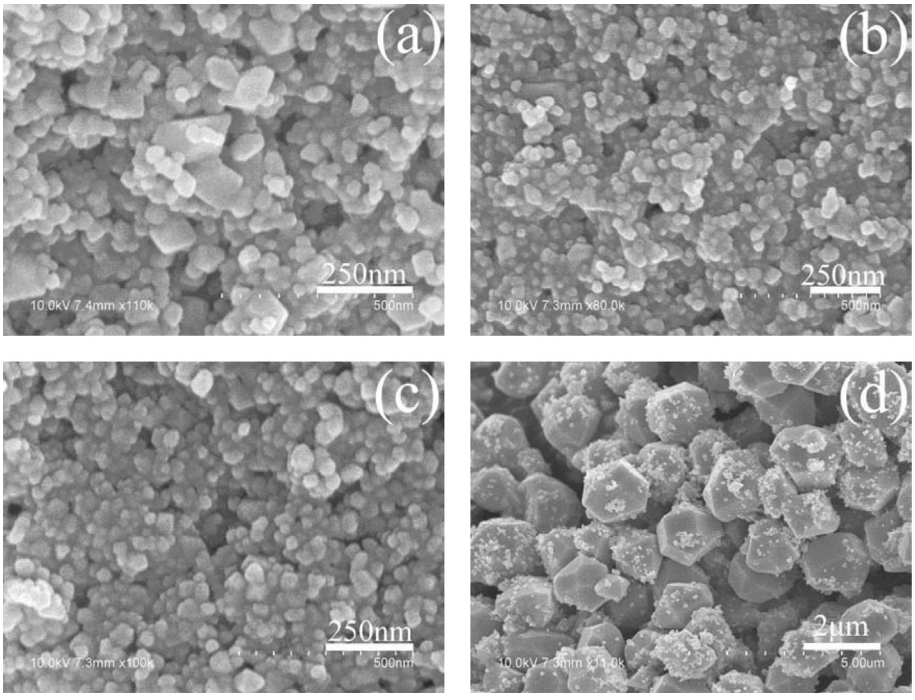

Figure 3 SEM images of the products with different volumes of glycerol: (a) 0 mL, (b) 5 mL, (c) 10 mL and (d) 15 mL.

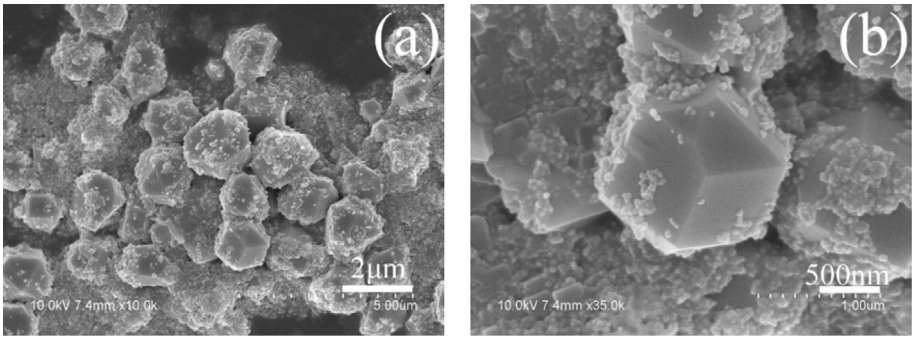

Figure 4 SEM images of the product at 150 °C for 24 h.

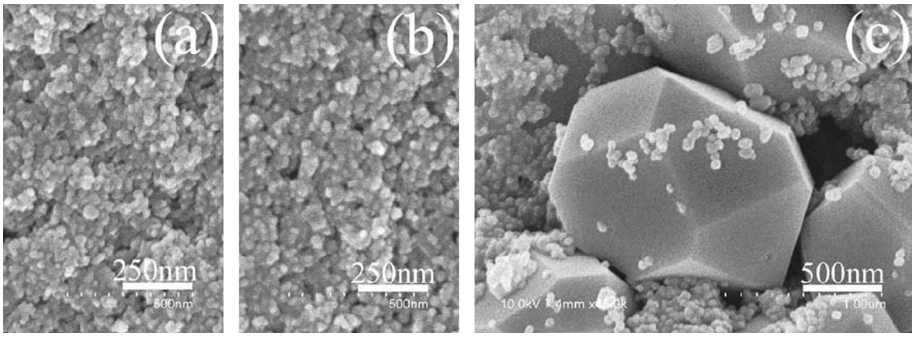

Figure 5 SEM images of the products with different reaction times: (a) 1 h, (b) 6 h and (c) 12 h.

to gain an insight into the formation process. When the reaction time was controlled at 1 h and 6 h, the product was composed of $PbMoO_4$ nanoparticles (Fig. 5a and b). On prolonging the reaction time to 12 h, $PbMoO_4$ polyhedrons and some nanoparticles were obtained (Fig. 5c). Further on increasing the reaction time to 24 h, $PbMoO_4$ polyhedrons with smooth surface were produced, accompanying the disappearance of the $PbMoO_4$ nanoparticles (Fig. 1). Based on

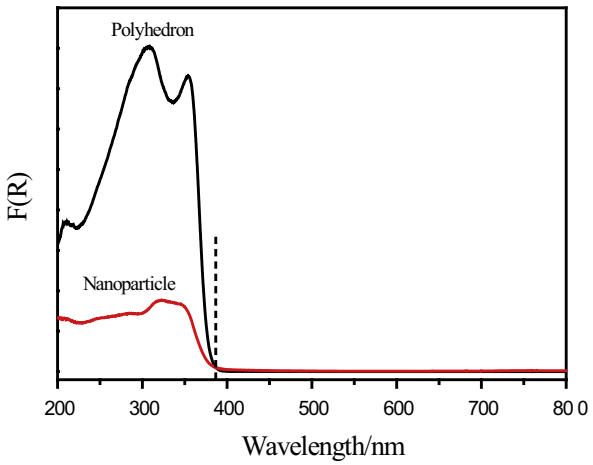

Figure 6 UV–vis diffuse reflectance spectra of the products with different morphologies.

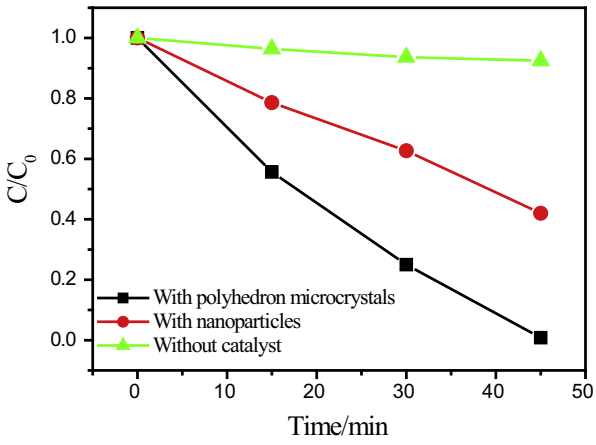

Figure 8 Photodegradation efficiencies of RhB as a function of irradiation time.

these, a probable formation mechanism of the $PbMoO_4$ polyhedrons is proposed. At an initial stage, small $PbMoO_4$ crystallites nucleate and further grow into nanoparticles (Fig. 5a and b). With the prolonging of reaction time, $PbMoO_4$ polyhedrons gradually form at the expense of the nanoparticles (Fig. 5c). Finally, the product is composed of $PbMoO_4$ polyhedrons with a smooth surface (Fig. 1). Ostwald ripening mechanism may account for the development of such polyhedrons [4].

UV–vis diffuse reflectance spectra of $PbMoO_4$ polyhedrons (with 20 mL of glycerol at 180 °C for 24 h) and nanoparticles (without glycerol at 180 °C for 24 h) are presented in Fig. 6. The wavelength at the absorption edge, λ, is determined as the intercept on the wavelength axis for a tangent line drawn on the absorption spectra. The absorption edge of both $PbMoO_4$ samples is 387 nm, corresponding to a band gap of ~3.21 eV, which is in good agreement with the reported value [15]. However, it should be noted that the polyhedrons possess higher light absorbance ability in the range from 387 to 200 nm than $PbMoO_4$ nanoparticles.

To demonstrate the potential application of these two kinds of $PbMoO_4$ micro/nanomaterials in the degradation of organic contaminants, the photocatalytic properties of $PbMoO_4$ with different morphologies were investigated by choosing the photocatalytic degradation of MO or RhB with high concentrations as a model reaction. Fig. 7a shows the photocatalytic degradation of MO on $PbMoO_4$ polyhedrons and nanoparticles, presenting the concentration changes of MO at 464 nm as a function of irradiation time during the degradation process. As is well known, the dye can undergo self-photolysis under UV-light irradiation. In our experiments, one can find that only 14% of MO can be photolyzed after 60 min reaction in the absence of photocatalyst. In contrast, almost 93% of MO has been photolyzed employing $PbMoO_4$ polyhedron microcrystals as photocatalyst in the same irradiation time. In the presence of $PbMoO_4$ nanoparticles, this decomposition percentage is 80%. These experimental results indicate that both $PbMoO_4$ products can greatly degrade MO and $PbMoO_4$ polyhedrons owing to their better degradation abilities. To a detailed analysis of the photocatalysis kinetics of the MO degradation in our experiments, we apply the pseudo-first order model as expressed by Eq. (1), which is generally used for photocatalytic degradation process if the initial concentration of the pollutant is low [28].

$$\ln(C_0/C) = kt \tag{1}$$

The C_0 and C are the concentrations of organic dye in solution at time 0 and t, respectively, and k is the pseudo first-order rate

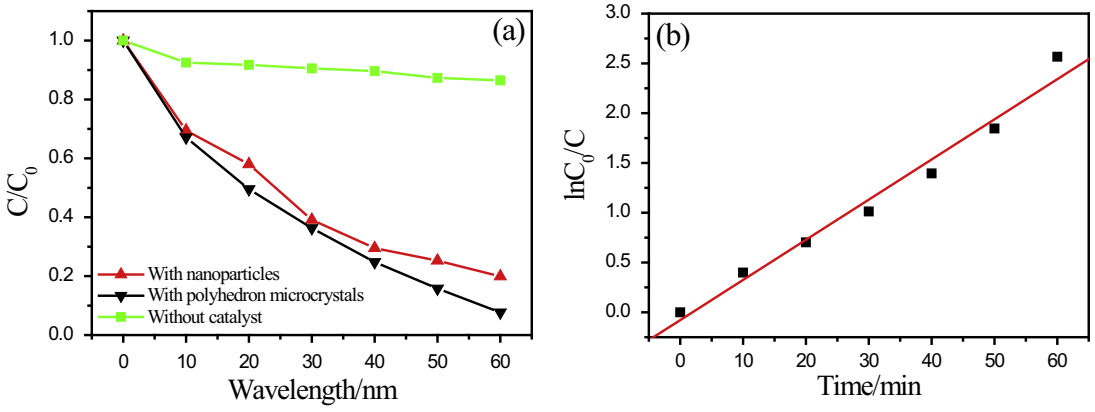

Figure 7 (a) Photodegradation efficiencies of MO as a function of irradiation time and (b) kinetics of MO decolorization with $PbMoO_4$ polyhedron microcrystals as photocatalyst.

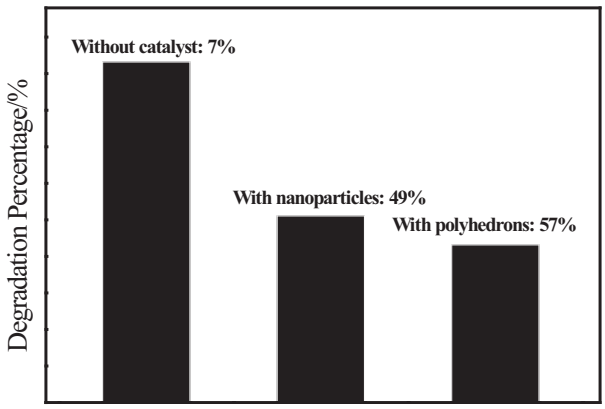

Figure 9 Photodegradation efficiencies of phenol solution after 3 h of UV-light irradiation.

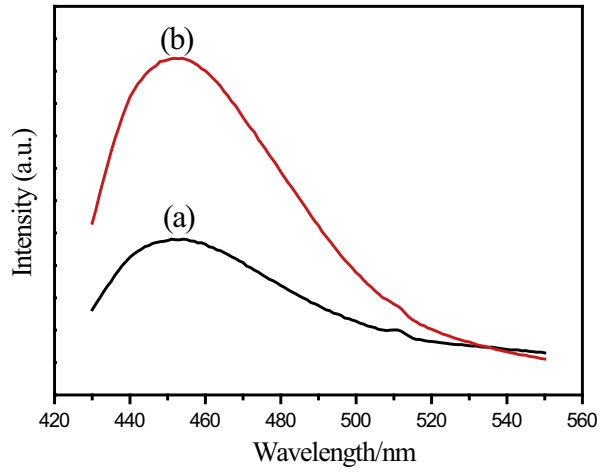

Figure 10 Photoluminescence spectra of the PbMoO4 polyhedron microcrystals (a) and nanoparticles (b).

constant. Fig. 7b is the photocatalytic reaction kinetics of MO degradation in solution on the basis of the data plotted in Fig. 7a employing $PbMoO_4$ polyhedrons as catalyst. As can be seen, a rather good correlation to the pseudo first-order reaction kinetics ($R > 0.99$) is found.

When RhB is used as a model pollutant, the two products also exhibit excellent photocatalytic activities for the degradation of RhB under UV light irradiation (Fig. 8). The above experiments indicate that the as-prepared $PbMoO_4$ samples are expected to be useful in water pollution control.

In order to understand that the degradation abilities of the products can be ascribed to direct or indirect photocatalysis, phenol in aqueous solution under UV light irradiation was also studied. TOC concentrations of phenol solutions were checked on a TOC analyzer. Fig. 9 displays the changes of the phenol concentration versus the reaction time over $PbMoO_4$ polyhedrons and nanoparticles, which clearly indicate that with identical UV light exposure, both samples show high photocatalytic activities and the decomposition percentages for $PbMoO_4$ polyhedrons and nanoparticles are 57 % and 49 %, respectively. Similarly, $PbMoO_4$ polyhedrons possess better degradation ability than nanoparticles.

Several reasons may account for the higher photocatalytic activity of $PbMoO_4$ polyhedrons than nanoparticles. Firstly, although $PbMoO_4$ nanoparticles owe higher BET surface areas (26.6 m^2/g) than polyhedrons (~0.0 m^2/g), the $PbMoO_4$ polyhedrons possess stronger light absorbance than nanoparticles, which may play an important role in the enhancement of photocatalytic activities [29,30,23]. Secondly, $PbMoO_4$ polyhedrons possess higher separation efficiency of photo-generated electron–hole pairs, which contributes to the better photocatalytic abilities. This point can be confirmed by the photoluminescence analysis. As is shown in Fig. 10, one can find that the photoluminescence intensity of nanoparticles is stronger than polyhedrons, which indicates that photo-generated charge of $PbMoO_4$ nanoparticles is easy to recombine and lead to relatively poor photocatalytic activities [17,25].

To further investigate the mechanism of the photocatalytic process over the $PbMoO_4$ polyhedron catalyst, quantities of different appropriate species scavengers such as isopropanol (IPA), sodium oxalate ($Na_2C_2O_4$) and benzoquinone (BQ) were introduced into the RhB solution prior to addition of the catalyst as scavengers of $^{\cdot}OH$, h^+ and $^{\cdot}O_2^-$, respectively [22]. Their concentrations were about 2.0 mM. The corresponding experimental results are shown in Fig. 11a. One can find that $Na_2C_2O_4$ and BQ had a strong influence on the degradation efficiency of RhB. However, the degradation rate of RhB hardly changes after the addition of IPA. The above

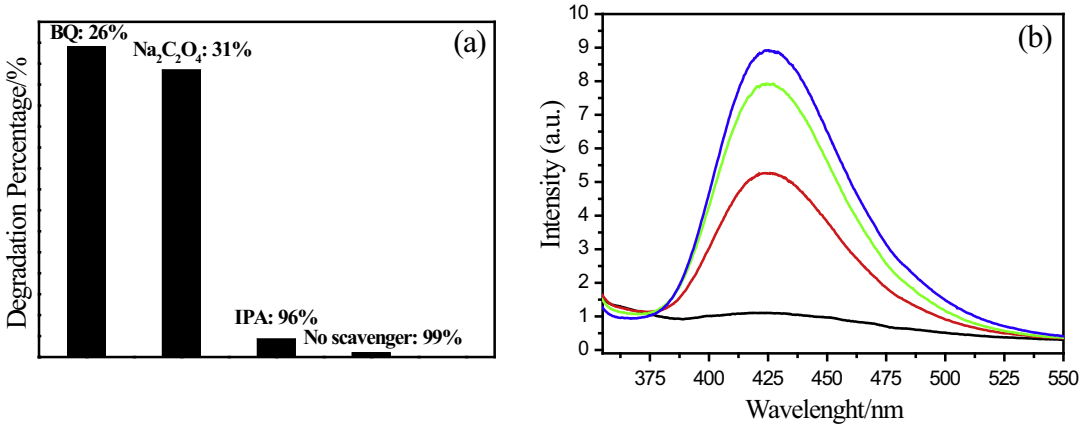

Figure 11 (a) Photocatalytic degradation of MO over the $PbMoO_4$ polyhedron microcrystals with or without quenchers under UV light irradiation; (b) $^{\cdot}OH$ trapping photocatalytic spectra of $PbMoO_4$ polyhedron microcrystals-TA suspension under UV light irradiation.

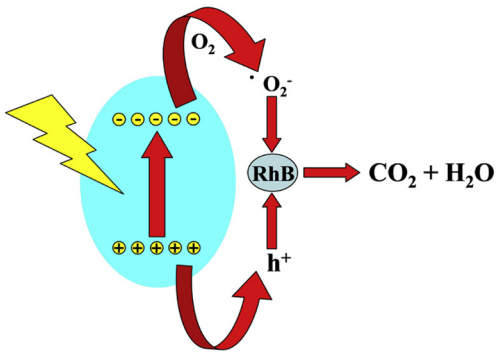

Scheme 1 Possible photocatalytic mechanism scheme of $PbMoO_4$ polyhedron microcrystals.

experimental results indicate that h^+ and $\cdot O_2^-$ played more important roles than ·OH in the photodegradation of RhB.

Moreover, terephthalic acid (TA) photoluminescence probing technique was introduced to further monitor the formation of ·OH on the surface of the photocatalysts [19,20]. The experimental procedure was similar as for the photocatalytic process, except that the RhB solution was replaced by a 5×10^{-4} M TA solution in 2×10^{-3} M NaOH solution. Fig. 11b shows the PL spectra changes observed during UV light irradiation of $PbMoO_4$ polyhedrons. The excitation wavelength is controlled at 315 nm. Obviously, the PL peak at about 425 nm gradually increased with the prolonging of irradiation time, which suggests the generation of ·OH radicals. Nevertheless, it should be noted that the intensity of the PL signal is comparatively weak relative to the previous report [3], which implies that only a small amount of ·OH is formed. Thus, it is reasonable to believe that ·OH may not be the main reactive species in the photocatalytic degradation process of RhB. In summary, the main reactive species involved in the degradation of RhB are h^+ and $\cdot O_2^-$. This experimental phenomenon is in good agreement with the reported literature [3]. A proposed photocatalytic mechanism for the degradation of RhB over the $PbMoO_4$ polyhedron catalyst is presented in Scheme 1.

4. Conclusion

In summary, we have developed a facile surfactant-free hydrothermal synthetic approach for the preparation of $PbMoO_4$ polyhedrons. Experimental results show that appropriate volume of glycerol, high reaction and long reaction time favor the formation of $PbMoO_4$ polyhedrons with smooth surface. Experiments indicate that $PbMoO_4$ polyhedrons possess better UV-light-driven photocatalytic activities, which can be ascribed to their higher light absorbance and separation efficiency of photo-generated electron–hole pairs. Compared to existing solution-phase synthetic methods, this work provides a facile, high-yield and low-cost pathway to synthesis of $PbMoO_4$ polyhedrons.

Acknowledgments

We gratefully acknowledge financial support from the Natural Foundation of Anhui Province (Nos. 1308085QB34 and 1208085QB27) and the National Natural Science Foundation of China (No. 21201006).

References

[1] V.M. Anandakumar, M. Abdul Khadar, Microhardness studies of nanocrystalline lead molybdate, Mater. Sci. Eng. A 519 (2009) 141.
[2] J.H. Bi, L. Wu, Y.F. Zhang, Z.H. Li, J.Q. Li, X.Z. Fu, Solvothermal preparation, electronic structure and photocatalytic properties of $PbMoO_4$ and $SrMoO_4$, Appl. Catal. B. 91 (2009) 135.
[3] J. Cao, B.Y. Xu, H.L. Lin, B.D. Luo, S.F. Chen, Novel heterostructured Bi_2S_3/BiOI photocatalyst: facile preparation, characterization and visible light photocatalytic performance, Dalton Trans. 41 (2012) 11482.
[4] M.H. Cao, H.Q. Lian, C.W. Hu, Ligand-assisted fabrication of hollow CdSe nanospheres via Ostwald ripening and their microwave absorption properties, Nanoscale 2 (2010) 2619.
[5] Y. Cheng, S.Y. Wang, D.Q. Chen, F. Bao, Evolution of single crystalline dendrites from nanoparticles through oriented attachment, J. Phys. Chem. B 109 (2005) 794.
[6] Y. Ding, S.H. Yu, C. Liu, Z.A. Zang, 3D architectures of iron molybdate: phase selective synthesis, growth mechanism, and magnetic properties, Chem. Eur. J. 13 (2007) 746.
[7] J.A. Dirksen, T.A. Ring, Fundamentals of crystallization: kinetic effects on particle size distributions and morphology, Chem. Eng. Sci. 46 (1991) 2389.
[8] R.P. Jia, Y.Q. Zhang, Synthesis and optical properties of $PbMoO_4$ nanoplates, Chin. Opt. Lett. 8 (2010) 1152.
[9] M. Hashim, C.G. Hu, X. Wang, X.Y. Li, D.L. Guo, Synthesis and photocatalytic property of lead molybdate dendrites with exposed (0 0 1) facet, Appl. Surf. Sci. 258 (2012) 5858.
[10] D.B. Hernández-Uresti, A. Martínez-de la Cruz, M. Torres-Martínez Leticia, Photocatalytic properties of $PbMoO_4$ synthesized by co-precipitation method: organic dyes degradation under UV irradiation, Res. Chem. Intermed. 38 (2012) 817.
[11] Z.P. Liu, J.B. Liang, S. Li, S. Peng, Y.T. Qian, Synthesis and growth mechanism of Bi_2S_3 nanoribbons, Chem. Eur. J. 10 (2004) 634.
[12] A. Phuruangrat, T. Thongtem, S. Thongtem, Synthesis of lead molybdate and lead tungstate via microwave irradiation method, J. Cryst. Growth 311 (2009) 4076.
[13] A. Phuruangrat, T. Thongtem, S. Thongtem, Analysis of lead molybdate and lead tungstate synthesized by a sonochemical method, Curr. Appl. Phys. 10 (2010) 342.
[14] J.C. Sczancoski, M.D.R. Bomio, L.S. Cavalcante, M.R. Joya, P.S. Pizani, J.A. Varela, E. Longo, M.S. Li, J.A. Andrés, Morphology and blue photoluminescence emission of $PbMoO_4$ processed in conventional hydrothermal, J. Phys. Chem. C 113 (2009) 5812.
[15] M. Shen, Q.G. Zhang, H. Chen, T.Y. Peng, Hydrothermal fabrication of $PbMoO_4$ microcrystals with exposed (0 0 1) facets and its enhanced photocatalytic properties, CrystEngComm. 13 (2011) 2785.
[16] T. Sugimoto, Preparation of monodispersed colloidal particles, Adv. Coll. Interf. Sci. 28 (1987) 65.
[17] J.T. Tang, Y. Liu, H.Z. Li, Z. Tan, D.T. Li, A novel Ag_3AsO_4 visible-light-responsive photocatalyst: facile synthesis and exceptional photocatalytic performance, Chem. Commun. 49 (2013) 5498.
[18] M.H. Ullah, K. ll, C.S. Ha, Preparation and optical properties of colloidal silver nanoparticles at a high Ag^+ concentration, Mater. Lett. 60 (2006) 1496.
[19] Q.J. Xiang, J.G. Yu, P.K. Wong, Quantitative characterization of hydroxyl radicals produced by various photocatalysts, J. Coll. Interf. Sci. 357 (2011) 163.
[20] Q.J. Xiang, J.G. Yu, W.G. Wang, M. Jaroniec, Nitrogen self-doped nanosized TiO_2 sheets with exposed {001} facets for

enhanced visible-light photocatalytic activity, Chem. Commun. 47 (2011) 6906.
[21] G.J. Xing, R. Liu, C. Zhao, Y.L. Li, Y. Wang, G.M. Wu, Photoluminescence and photocatalytic properties of uniform $PbMoO_4$ polyhedral crystals synthesized by microemulsion-based solvothermal method, Ceram. Int. 37 (2011) 2951.
[22] Y. Xu, S.C. Xu, S. Wang, Y.X. Zhang, G.H. Li, Citric acid modulated electrochemical synthesis and photocatalytic behavior of BiOCl nanoplates with exposed {001} facets, Dalton Trans. 43 (2014) 479.
[23] M.H. Yang, Y.J. Xu, Selective photoredox using graphene-based composite photocatalysts, Phys. Chem. Chem. Phys. 15 (2013) 19102.
[24] Q.Y. Yu, C.Y. Liu, Z.Y. Zhang, Y. Liu, Facile synthesis of semiconductor and noble metal nanocrystals in high-boiling two-phase liquid/liquid systems, J. Phys. Chem. C 112 (2008) 2266.
[25] C.L. Yu, F.F. Cao, X. Li, G. Li, Y. Xie, J.C. Yu, Q. Shu, Q.Z. Fan, J.C. Chen, Hydrothermal synthesis and characterization of novel $PbWO_4$ microspheres with hierarchical nanostructures and enhanced photocatalytic performance in dye degradation, Chem. Eng. J. 219 (2013) 86.
[26] L. Zhang, X.F. Cao, Y.L. Ma, X.T. Chen, Z.L. Xue, Microwave-assisted solution-phase preparation and growth mechanism of $FeMoO_4$ hierarchical hollow spheres, CrystEngComm. 12 (2010) 207.
[27] L. Zhang, X.F. Cao, Y.L. Ma, X.T. Chen, Z.L. Xue, Pancake-like $Fe_2(MoO_4)_3$ microstructures: microwave-assisted hydrothermal synthesis, magnetic and photocatalytic properties, New J. Chem. 34 (2010) 2027.
[28] L. Zhang, X.F. Cao, X.T. Chen, Z.L. Xue, BiOBr hierarchical microspheres: microwave-assisted solvothermal synthesis, strong adsorption and excellent photocatalytic properties, J. Coll. Interf. Sci. 354 (2011) 630.
[29] N. Zhang, S.Q. Liu, Y.J. Xu, Recent progress on metal core@semiconductor shell nanocomposites as a promising type of photocatalyst, Nanoscale 4 (2012) 2227.
[30] N. Zhang, Y.H. Zhang, Y.J. Xu, Recent progress on graphene-based photocatalysts: current status and future perspectives, Nanoscale 4 (2012) 5792.
[31] L. Zhou, W.Z. Wang, H.L. Xu, S.M. Sun, Template-free fabrication of $CdMoO_4$ hollow spheres and their morphology-dependent photocatalytic property, Cryst. Growth Des. 8 (2008) 3595.
[32] W.W. Zhou, B. Yan, C.W. Cheng, C.X. Cong, H.L. Hu, H.J. Fan, T. Yu, Facile synthesis and shape evolution of highly symmetric 26-facet polyhedral microcrystals of Cu_2O, CrystEngComm. 11 (2009) 2291.